RSC Advances

ROYAL SOCIETY OF CHEMISTRY

www.rsc.org/advances

N^1-(3-trimethoxysilylpropyl)diethylenetriamine Grafted KIT-6 for CO_2/N_2 Selective Separation

Rupak Kishor*, Aloke Kumar Ghoshal

Department of Chemical Engineering, Indian Institute of Technology Guwahati,

Guwahati-781039, Assam, India

Abstract

In the present study N^1-(3-trimethoxysilylpropyl)diethylenetriamine was grafted on various ordered and commonly used mesoporous silica namely MCM-41 (2.2 nm), SBA-15 (6.6 nm) and KIT-6 (6.6 nm) in both anhydrous and aqueous conditions for CO_2/N_2 adsorption. The structural and physical properties before and after grafting were analyzed by nitrogen adsorption/desorption, X-ray diffraction and electron microscopy techniques. The uptake capacities of three-dimensional K30T and WK30T were 1.89 and 2.59 mol CO_2/kg of adsorbent, respectively at 30 ºC which are significantly higher than MCM-41 and SBA-15 based adsorbents. Analysis of enthalpy of CO_2 adsorption, confirmed the adsorption in amine functionalized adsorbents by both chemical and physical interactions. Outstanding equilibrium CO_2/N_2 selectivity of functionalized KIT-6 over MCM-41 and SBA-15 opens up its practical applicability through stable performance in several adsorptions/desorption cycles.

Keywords

Adsorbent, Aminosilane, CO_2/N_2 adsorption, Grafting, Ordered mesoporous silica, Selectivity

Corresponding author e-mail: rupak.k@iitg.ernet.in

1. Introduction

Increasing trends of CO_2 concentration in the atmosphere is creating alarming conditions in the form of global warming across the globe. Especially in last few decades, the rate of CO_2 emission in the form of flue gas is drastically increased from large anthropogenic source, particularly a coal based thermal power plant. This is possibly for industrialization and growth in energy demand across the globe.[1,2] As a result, the atmospheric CO_2 concentration increased from ~315 ppm in 1958 to ~400 ppm in 2015. Higher CO_2 concentrations have led to several environmental issues and therefore, reducing CO_2 emissions from the large anthropogenic source is urgently required.

In order to control the CO_2 concentration in the atmosphere, carbon capture sequestration and utilization (CCSU) is a promising technology and is becoming indispensable to develop an efficient and cost effective separation process.[3] Basic monoethanolamine (MEA), diethanolamine (DEA) and mixed amines based absorption is in commercial operation throughout the world.[3,4] But, solid sorbent based separation process could be a potential alternative and a lot of innovative work has been carried out to develop highly CO_2/N_2 selective adsorbents. CO_2 from the anthropogenic source may be separated by a verity of solid physisorbents like zeolite,[5] porous carbon,[6,7] metal-organic frameworks (MOFs),[3,8–12] covalent organic frameworks (COFs)[13], polymer[14] and chemisorbents like alkali functionalized mesoporous silica and metal carbonates.[15–29] Microporous metal-organic frameworks shows very high sorption capacities and selectivity,[8–12] but susceptibility to moisture[8] demanding for further research for better alternatives. Alkali based metal carbonate (M_2CO_3, where M = Mg, Na, Cu, Zn etc.) and amine functionalized ordered mesoporous silica (OMSs) based regenerable solid sorbent are good alternatives over physisorbents for CO_2 sorption from flue gas.[15–17] Lee et al.[16–17] synthesized excellent adsorbent with 87 – 119 mg CO_2/g sorption capacity at 60 ºC and 1 bar by impregnation of potassium carbonate in ZrO_2, AC, TiO_2, Al_2O_3, MgO, SiO_2 and various zeolites. However, regeneration

temperature (130 – 400 ºC) and poor cyclic performance of adsorbents became less favourable for CO_2 capture. Amines are highly selective towards CO_2 via. carbamate formation in low partial pressure as well as stable and easily regenerable at moderate temperature even in moist environment.[18–29] Aminosilane functionalized OMS is a suitable alternative for CO_2 sorption from anthropogenic source.

Since after the discovery of OMS by Mobil scientists in the early 1990[s],[30] other OMSs like SBA-15[22,27] (hexagonal), KIT-6[28] (cubical), MCF[31] (disordered) and MSU[32] (hexagonal disordered) were also discovered. Due to high specific surface area (> 600 m^2/g) and pore volume (> 0.5 cc/g), they have attracted world-wide researcher's interest in various applications like catalysis,[33] nano-science[34] and drug delivery[35] by decorating the surface with organosilane. Yokoi at al.[19] synthesized the functionalized MCM-41 by direct co–condensation reaction with aminosilane and silica source during synthesis as well as by post grafting method. Among these, amine functionalized OMSs received the attention of a large community in CO_2 capture application. More recently, Linneen et al.[25] grafted mono, di and triaminosilane on silica aerogel with larger pore size (42.7 nm) and pore volume (4.2 cc/g) and studied the CO_2 adsorption performance. It was found that, the adsorption capacity was increased with increasing amine chain length and maximum for triaminosilane grafted aerogel (1.64 mol CO_2/kg at 25 ºC and 1 bar). Hiyoshi et al.[21] improved the aminosilane loading by improving the surface properties of SBA-15 by boiling in water followed by post grafting. Sayari et al.[36] reported that adsorption is directly associated to amine content present in the adsorbent. Zeleňák et al.[29] showed the three dimensional with inter connected porous structure provides faster response during CO_2 uptake than long hexagonal porous structure. We recently demonstrated that aminopropyl grafting in aqueous solution was more significant for aminosilane loading as well as CO_2 adsorption over anhydrous grafting.[29]

The physical properties of the support and method of grafting play an important role in the performance of the adsorbent. In the present study, we focus on in-depth understanding in

designing the highly CO_2/N_2 selective aminosilane grafted adsorbent. In view of exploiting the presence of more amino nitrogen for capturing more CO_2, this study attempted selection of the best one from the group of commonly used mesoporous adsorbents. In the process of investigation, the traditional MCM-41, SBA-15 and KIT-6 mesoporous silica were synthesized by liquid crystal templating mechanism. Thereafter, they were functionalized with N^1-(3-Trimethoxysilylpropyl)diethylenetriamine by grafting method in the anhydrous and aqueous solution. The adsorbents were characterized by a various analytical and spectroscopic techniques and also by CO_2/N_2 uptake measurements under different conditions. The adsorption capacity was compared to decide upon the best support for CO_2 adsorption. The variations in adsorption capacities are also elucidated by grafting mechanism and structural properties of the adsorbents.

2. Experimental

Materials

The chemicals pluronic EO–PO–EO triblock copolymer (P123, Sigma-Aldrich), N^1-(3-Trimethoxysilylpropyl)diethylenetriamine (TMPTA, Sigma) cetrimide (CTAB, Merck), tetraethyl orthosilicate (TEOS, Sigma-Aldrich), ammonia solution (NH_3 25%, Merck), hydrochloric acid (HCl, 35%, Merck), 1–butanol (BuOH, Merck), ethanol (EtOH, Merck), and anhydrous toluene were used without any further treatment.

Synthesis of ordered mesoporous silica

MCM-41 was synthesized by following procedure:[37] 2.0 g CTAB was dissolved in 120 mL Millipore purified water. After complete dissolution, 9.0 mL of NH_3 was added. The 10 mL of TEOS was added drop wise in solution and stirred for another 12 h at room temperature. The white solid product was filtered, washed with distilled water and dried at 100 ºC for 24 h. Surfactant free MCM-41 was obtained after calcination at 550 ºC for 5 h.

SBA-15 was synthesized by modified procedure:[22] 4.0 g of P123 was dissolved in 144 mL of 1.7 N HCl at 40 ºC. After it became homogeneous, 8.0 g TEOS was added in the solution and stirred for another 24 h at 40 ºC. The resulting mixture was transferred in Teflon lined autoclave and aged at 100 ºC for 24 h. The white solid product was obtained by filtration and dried at 100 ºC for 24 h. Surfactant free SBA-15 was obtained after calcination at 550 ºC for 5 h.

KIT-6 was synthesized as earlier reported procedure.[28] In typical synthesis, 4.0 g of P123 was dissolved in a mixture of 144 mL water and 7.9 g HCl at 40 ºC. Next, 4.0 g of 1-butanol was added in the solution and mixed for another 1 h. The 8.6 g of TEOS was added in the solution and continuously stirred for 24 h at 40 ºC. Resulting slurry was transferred into Teflon lined autoclave and hydrothermally treated at 100 ºC for 24 h. The white solid product was obtained after filtration of solution and dried in hot air oven at 100 ºC. Surfactant free KIT-6 was obtained after calcination at 550 ºC for 5 h.

Synthesis of aminosilane grafted OMSs

OMSs was functionalized with N^1-(3-Trimethoxysilylpropyl)diethylenetriamine by post grafting method.[23] Before grafting, 1.0 g of OMS (MCM-41, SBA-15 and KIT-6) was dried at 120 ºC in vacuum to remove the pre adsorbed moisture. In anhydrous grafting, 1.0 g of OMS was dispersed in 150 mL toluene and stirred for 1 h to become homogeneous. Then, 'x' mL of TMPTA was added in the solution and refluxed at 85 ºC in stirring condition for 24 h. The TMPD grafted OMS was filtered and washed repeatedly with toluene and ethanol. The solid product was dried at 80 ºC in high vacuum for 16 h and stored for further analysis. The obtained samples are designated as M'x'T, S'x'T and K'x'T of MCM-41, SBA-15 and KIT-6, respectively of base material. In aqueous grafting, after complete dispersion of OMS in toluene, 0.10 mL Millipore purified water was added and stirred for 3 h to modify the silica surface. The further steps were similar as discussed in dry grafting. The resulting samples are denoted as WM20T, WS20T and WK30T.

Material characterization

High resolution X-ray powder diffraction spectra were recorded by Bruker D8 advance diffractometer using CuKα radiation operating at 40 kV and 40 mA. Surface micrographs of synthesized OMSs were recorded by field emission scanning electron microscope (FESEM) (Zeiss, Sigma). Transmission electron micrograph (TEM) was recorded using a Jeol (JEM 2100, 200 keV) instrument. Nitrogen adsorption/desorption isotherm was recorded on Quantachrome automated volumetric gas sorption analyzer (autosorb iQ) at –196 ºC. Before analysis, samples were degassed at 120 ºC for 3 h in ultra-high vacuum. Specific surface area (S_{BET}) was calculated by Brunauer–Emmett–Teller (BET) method. The pore volume (v_t) was calculated by volume adsorbed basis at relative pressure 0.99. Pore size distribution was calculated by Barrett-Joyner-Halenda (d_{BJH}) method. Thermal analysis and aminosilane present in the adsorbents were analyzed by thermogravimetry (TG, Netzsch) analyzer.

CO_2/N_2 adsorption

CO_2/N_2 adsorption measurements were performed in high pressure volumetric gas adsorption apparatus (iSorbHP1-XKRLSPN100). A sample weight of ~250 mg was loaded into a sample holder and fitted with instrument. Before analysis, pre-adsorbed moisture and gases were removed by degassing the adsorbent at 110 ºC for 3 h in ultra-high vacuum and measured the actual weight of adsorbent. CO_2/N_2 adsorption measurement was conducted at 30, 45, and 60 ºC. The adsorbate gases, carbon dioxide (CO_2, 99.999%) and nitrogen (N_2, 99.999%) were obtained from Assam air product.

3. Results and discussion

Characterisation of the aminosilane grafted OMSs

The small angle X-ray diffraction patterns before and after TMPTA grafted MCM-41, SBA-15 and KIT-6 are shown in Fig. 1. In diffraction spectra, peaks observed at 2.6º (100), 0.90º (100) and 0.93º (211) for MCM-41, SBA-15 and KIT-6 mesoporous silica, receptively clearly indicates the synthesized OMSs are highly ordered in nature with corresponding hexagonal, hexagonal and la3d bicontinuous cubic lattice structure.[26–30] Fig. 2 shows the corresponding FESEM and TEM micrograph of pure MCM-41, SBA-15 and KIT-6. As seen in Fig. 2(a), MCM-41 exhibits monodispersed thin platelets with average particle size ~ 0.6μm.[37] Fig. 2b shows that synthesized SBA-15 is a road shaped particles structure in a highly ordered bundle.[38] KIT-6 exhibits as a particle with average size ~1 μm as shown in Fig. 2c. TEM micrographs of MCM-41, SBA-15 and KIT-6 clearly show the highly ordered structure of the synthesized material as reported in literature.[27–30] After grafting of TMPTA, peak intensity is significantly reduced in MCM-41 and sparsely reduced in SBA-15 and KIT-6 (Fig. 1). This is possibly due to complete pore filling in MCM-41 and partial pore filling in SBA-15 and KIT-6.[39] In addition, the peaks (110, 200), (110, 200) and (211) are diminishing after grafting of TMPTA in MCM-41, SBA-15 and KIT-6, respectively (Fig. 1). Thus, with increasing amine concentration in the solution, peak intensity decreased in all the adsorbents. In case of aqueous grafted adsorbent (Fig. 1), intensity of the major peak drastically reduced due to higher aminosilane loading.[25,28,36]

The nitrogen adsorption/desorption isotherm and pore size distribution of pure and aminosilane grafted OMSs are shown in Fig. 3 and physical properties are summarized in Table 1. All the OMSs demonstrate the type IV isotherm which is general characteristic of mesoporous (2–50 nm) material.[22,23,28,30] However, SBA-15 and KIT-6 shows the Type H1 hysteresis loop, which is characteristic of material with interconnected large cylindrical pore geometry and high degree of pore size uniformity.[40] However, MCM-41 does not show any hysteresis, which is mainly for narrow slit like pores present in the material and also pore size close to micropore range.[40] The specific surface area (S_{BET}) of mesoporous MCM-41 (2.2 nm), SBA-15 (6.6 nm) and KIT-6 (6.6

nm) was 1492, 857 and 860 m^2/g, respectively. After anhydrous aminosilane grafting on MCM-41, S_{BET} and pore volume are sharply reduced whereas S_{BET} of SBA-15 and KIT-6 approximately become $2/5^{th}$ of the original. This is obviously caused by the aminosilane grafting in the channels and internal mesoporous surface. But, approximately 50% of the pore volume of SBA-15 and KIT-6 remain empty. The surface area and pore volume of MCM-41, SBA-15 and KIT-6 are sharply reduced after aqueous aminosilane grafting (Table 1) and is due to higher amount of aminosilane grafting in presence of water. It may be noticed that, pore diameters of hexagonal MCM-41 and SBA-15 are highly reduced after aqueous aminosilane grafting whereas that of KIT-6 is not much affected. This is because of the presence of inter-connected porous channels in KIT-6.

FTIR analysis

The mechanism of aminosilane grafting over OMSs and CO_2 interaction with functionalized adsorbent is discussed through the IR–spectra as shown in Fig 4. Surface properties of MCM-41, SBA-15 and KIT-6 before grafting are compared using IR- spectra. In all the OMSs, a peak with a wide shoulder 3750 – 3400 cm^{-1} ascribes the presence of hydrogen-bonded silanol group (Si–OH) present on the surface.[41] Other peaks at 1250 – 1040 cm^{-1}, and ~ 799 cm^{-1} assign the asymmetric and symmetric stretching vibration of Si–O–Si silanol bridge. The peaks at 960 cm^{-1} and ~1620 cm^{-1} represent the free silanol groups and adsorbed water present on the silica surface.[33,42] After TMPTA grafting in OMSs, some new peaks evolved and some peaks disappeared in the spectra. The peak corresponds to 960 cm^{-1} was completely disappeared in the aminosilane grafted adsorbents because of grafting of aminosilane with the free silanol group present on the surface. The band at 2940 – 2880 cm^{-1} and 1410 cm^{-1} attributed to C–H and C–N stretching of aminosilane, respectively.[23,33,43] The peaks at 1630, 1580 and 1309 cm^{-1} are associated with chemical reaction between CO_2 and amine and formation of ammonium ions (NH_3^+), carbamate $(C{=}O{=}C)^-$ and $NCOO^-$ skeletal vibration, respectively.[43]

CO_2/N_2 adsorption on MCM-41, SBA-15 and KIT-6

The selection of appropriate mesostructured support can substantially reduce the size of the capture equipment and the cost. The CO_2 sorption capacity of sorbent is a primary objective in designing the separation process. Thus, in the present case, initially CO_2 adsorption was performed on pure OMSs at different temperatures to understand the effect of aminosilane loading. Before adsorption experiment, OMSs were degassed at 150 ºC for 3 h in ultra-high vacuum to remove the pre–adsorbed moisture and CO_2. The CO_2 adsorption isotherms on MCM-41, SBA-15 and KIT-6 at different temperatures 30, 45 and 60 ºC under pressure range up to 1 bar are shown in Fig. 5. The equilibrium adsorption capacity (q_e) almost linearly increases with increasing the pressure over all the OMSs. The following trend of q_e is observed for different OMSs: SBA-15(0.74 mol CO_2/kg) > KIT-6 (0.64 mol CO_2/kg) > MCM-41 (0.56 mol CO_2/kg) at 30ºC and 1 bar. The lowest q_e of MCM-41 even after the highest S_{BET} compared to SBA-15 and KIT-6 is possibly for different surface properties. SBA-15 (3.4 – 8.5 OH/nm^2)[22] contains more surface silanol than MCM-41 (2.5 – 3.0 OH/nm^2),[41] that resulted in the highest q_e. In case of KIT-6, possibly contains intermediated number of silanol groups on the surface. A known fact, the adsorption capacity is strongly influenced by temperature. The amount of CO_2 adsorbed on MCM-41 is decreased with increase in temperature and similar trends are observed with SBA-15 and KIT-6 as shown in Fig. 5.[38]

The N_2 adsorption isotherm on MCM-41, SBA-15 and KIT-6 under pressure range 1 bar is shown in Fig 5. The q_e is linearly increases with pressure and as following the order MCM-41 (0.04 mol N2/kg) ~ SBA-15 (0.04 mol N_2/kg) < KIT-6 (0.05 mol N_2/kg) at 30 °C and 1 bar.

Effect of aminosilane concentration

To understand the effect of aminosilane concentration in the solvent on grafting capacity as well as on q_e, a series of experiments were performed by varying the TMPTA to OMSs ratio and results

are summarized in Fig. S1. The hexagonal structured MCM-41 and SBA-15 show maximum CO_2 q_e for 2:1 (TMPTA: OMS) ratio. But, in case of three dimensional KIT-6, 3:1 (TMPTA: OMS) ratio gives maximum adsorption capacity. This q_e is reduced marginally with higher concentration. The TMPTA intensity at the internal surface is increased but the active site is reduced due to overlapping with each other.[25,28,44] The degree of grafting on OMS is in the following order KIT-6 > SBA-15 > MCM-41. Diffusional resistance and pore blocking can control the movement of amine into the interior of the pore. Presence of interconnected pore in KIT-6 reduces the diffusional resistance and thereby reduces the hindrance of the movement of amine for grafting.[29] This in turn reduces the pore blocking also.

Extracted information from anhydrous grafting is used further for aqueous grafting as the latter is a more efficient way to graft the aminosilane in OMSs. In the present study, water to OMSs ratio (0.1) in solution were maintained during grafting of aminosilane. The q_e of aqueous grafted adsorbent (WM20T and WS20T) was reduced to 0.66 and 0.64 mmol CO_2/g from 1.36 (M20T) and 1.54 (S20T) mmol CO_2/g of adsorbent as shown in Fig. 6. Whereas, the q_e of WK30T were increased from 1.89 mmol CO_2/g to 2.59 mmol CO_2/g at 30 ºC and 1 bar. This suggests that the surface architecture and mesopore size of OMS affects the degree of silylation and q_e. However, aminosilane loading was higher during aqueous grafting than anhydrous as explained in the section below.[25,36] The reduction in q_e of aqueous grafted adsorbents corresponds WM20T and WS20T is possibly due to plugging the pores of MCM-41 and SBA-15 through inter aminosilane condensation reaction.

Effect of temperature on CO_2/N_2 adsorption

Sorption temperature as well as capacity of adsorbent are essential parameters in designing the adsorption process. In the present study, CO_2/N_2 adsorption isotherm on M20T, S20T and K30T at (30, 45, and 60) ºC in the pressure range of 0 – 1.0 bar were performed and the results are depicted

in Fig. 7. The CO_2 q_e of all the aminosilane grafted adsorbents progressively decreases with increasing the temperature. The maximum q_e is obtained at 30 ºC as per the following order K30T (1.89 mol CO_2/kg) > S20T (1.54 mol CO_2/kg) > M20T (1.36 mol CO_2/kg). When the temperature is increased to 60 ºC, q_e becomes 1.63, 1.04, 1.01 mmol CO_2/g of K30T, S20T and M20T respectively at 1 bar.

The similar trends of CO_2 adsorption isotherm over aqueous grafted adsorbent (WK30T) were observed at different temperatures. However, reduction in CO_2 adsorption capacity of WK30T with temperature is much less as shown in Fig. 8. The q_e is 2.59, 2.47 and 2.38 mol CO_2/kg at 30, 45 and 60 ºC, respectively. The values are much higher than M20T and S20T. Table 2, summarized the maximum q_e and compared with other TMPTA grafted mesoporous silica. As can be seen from the table, WK30T is better performing with respect to other adsorbents. It is further observed that, larger pore mesoporous silica gives better q_e after TMPTA aqueous grafting compared to smaller size mesoporous silica.[45–48]

Multi temperature Dual-site Langmuir (DSL) model[6,12] explained in the supplementary information (ESI) is used to describe the CO_2 adsorption behaviour on TMPTA grafted adsorbents at different temperatures. The DSL model (continuous line) (Figs. 7 and 8) show excellent agreement with the experimental data (solid Points) at different temperatures.

The reduction in CO_2 adsorption capacity over amine grafted adsorbents can be explained by the classical adsorption mechanism. The CO_2 adsorption on amine grafted OMSs is an exothermic process and it becomes more favourable at lower temperature. Compared with some other aminosilane functionalized adsorbent, similar behaviour was observed in the present study.[23,27,48] Whereas, Sayari et al.[49] showed the q_e of TMPTA grafted PE-MCM-41 was somewhat increased with increasing the temperature. It facilitates the diffusion of CO_2 in aminosilane layer with temperature and increased the active amine sites for interaction. The similar adsorption behaviour

was also observed in polyamine impregnated mesoporous silica.[31,32,39] But in the present case, CO_2 diffusion in aminosilane layer with temperature is dominated by the desorption process and reduced the capacity at higher temperature.

During grafting, aminosilane cover a fraction of the surface.[46] Hereafter, sorption capacity of amine functionalized adsorbent is combined effect of chemical and physical adsorption.[49] In a low CO_2 partial pressure (~ till 0.15 bar), the sorption capacity of M20T, S20T and K30T increased sharply and it was mainly for chemical adsorption between CO_2 and grafted aminosilane.[32,39] Moreover, at higher CO_2 partial pressure sorption capacity gradually increases with pressure and it was probably for physical adsorption with the surface.[49]

Low q_e of N_2 indirectly indicates the high CO_2/N_2 selectivity of the adsorbent. Figs. 7d, 7e and 7f show the effect of temperature (30, 45 and 60 ºC) on N_2 adsorption performance over M20T, S20T and K30T. Nitrogen q_e at 30 ºC and 1 bar was 0.019, 0.012 and 0.011 mol N_2/kg of M20T, S20T and K30T adsorbent, respectively. There was no major difference in q_e of all the adsorbents and moreover not much affected with adsorption temperature. In case of aqueous grafted WK30T, q_e was 0.013, 0.008 and 0.007 mol N_2/kg adsorbent at 30, 45 and 60 ºC at 1 bar, respectively as shown in Fig. 8b. The adsorption capacity of N_2 in amine grafted mesoporous silica is much lower than other adsorbents like MOF and polymeric adsorbent,[12,14,50] which makes amine functionalized mesoporous silica a lucrative option over other adsorbents. Additionally, the q_e of CO_2 is much higher than that of N_2 at all temperatures in all the adsorbents because of the greater quadrupole moment and polarizability of CO_2 (4.30×10^{-26} esu cm^2 and 29.11×10^{-25} cm^3, respectively) than N_2 (1.52×10^{-26} esu cm^2 and 17.403×10^{-25} cm^3, respectively).[51]

The important parameter before selection of any adsorbent is the selectivity. It is defined by $S_{x/y} = (q_{ei}/q_{ej})/ (p_i/p_j)$; Where q_{ej}, q_{ej} and p_i, p_j are the amount adsorbed and corresponding partial pressure for component i and j, respectively.[52] The CO_2 and N_2 (~ 15: 85) is a major component of flue gas

emitted from coal based thermal power plant. In the present study, on the basis of this composition the selectivities at 30 ºC are 14, 23 and 15 of MCM-41, SBA-15 and KIT-6, respectively. After TMPTA grafting, selectivity is improved to 491, 635, 793 and 873 of M20T, S20T, K30T and WK30T, respectively.

Enthalpy of adsorption

Enthalpy of adsorption (ΔE_{ads}) is calculated by Clausius–Clapeyron relation.[12] The $-\Delta E_{ads}$ values for CO_2 on pure MCM-41, SBA-15 and KIT-6 are ca. 18, 20 and 18 kJ/mol and constant with loading.[23,26] At zero coverage of CO_2 adsorption (Fig. 9) over TMPTA grafted adsorbents; $-\Delta E_{ads}$ value is much higher than the pure OMSs.[22,26] This is due to the chemical interactions between CO_2 and amine present on the surface as earlier confirmed by several authors.[22–24,49] The $-\Delta E_{ads}$ values are summarized in the Table. 3. A sharp reduction in enthalpy is observed with increase in loading at higher pressure. It confirms fact that the amine functionalized silica contains two different types of site for CO_2 adsorption as earlier explained by Sayari et al.[45] which is namely amine and bare silica surface. In the initial phase higher enthalpy value is for major contribution from chemisorption with amine and later lower for major contribution from physical interaction with the surface because of exhaustion of amine.

TGA analysis

The amount of TMPTA present in the adsorbents was analyzed by TG analysis.[24,42] Fig. S2 (ESI) shows the TG curves of aminosilane grafted MCM-41, SBA-15 and KIT-6 and the corresponding differential thermal gravimetric (DTG) curves are shown in Fig 10. TG curves clearly show that the organic aminosilane completely degrade within 750 ºC. A sharp weight loss in all the adsorbents is observed in the initial temperature range 30 – 150 ºC, which is attributed to the loss of moisture and adsorbed gases. The three peaks observed in Fig. 10 in the ranges (150 – 250), (250 – 500) and (500 –750) ºC are due to decomposition of grafted aminosilane.[24,36,42] The

corresponding amine group numbers (mol N/kg-adsorbent) are summarized in Table 3. The amine groups available for CO_2 during adsorption is the highest in KIT-6 and the least in MCM-41 for both dry and anhydrous grafted adsorbents. During grafting in MCM-41 and SBA-15 with cylindrical pore mouth gets easily plugged by TMPTA. But in KIT-6, interconnected channel provides better surface accessability for grafting of guest molecule and accommodate higher amount of amine. The similar phenomenon was also reported by Zeleňák et al.[29] with aminopropyl grafting over different porous structures.

Amine efficiency is the ratio of CO_2 adsorbed (mol CO_2/kg) to amine group number (mol N/ kg) present in the adsorbent.[27,47,48] Hence, theoretical maximum possible amine efficiency is 0.5. TMPTA consists of one primary amine and two secondary amines. Primary and secondary amine of TMPTA reacts with CO_2 and formed carbamate with zwitterion intermediate,[27] where two amines reacts with one molecule of CO_2 under dry condition. Efficiency of grafted aminosilane in CO_2 adsorption increases with increase in the pore diameter of OMSs and it follows the order K30T > S20T > M20T. In case of hexagonal aqueous grafted adsorbents (WM20T and WS20T), efficiency decreased sharply even after higher amine loading. This indicates that the hexagonal pore has a diffusional limitation for CO_2 adsorption possibly due to pore blocking by condensation reactions between aminosilanes during grafting (Scheme 1). The similar trends were observed by several authors in recent study over amine functionalized adsorbent.[39,44] In case with WK30T, amine group number and CO_2 adsorption capacity proportionally increased. It is due to the mesoporous inter connected channels present in KIT-6 thus, reducing the said limitation.

Grafting mechanism

The main prerequisite in developing an efficient amine functionalized adsorbent is the selection of base mesoporous silica. In the present study, we grafted the aminosilane on high surface area OMSs with different structure (hexagonal, cubical), pore size and pore volume. The q_e of amine

functionalized adsorbent is directly associated with assessable amine groups for CO_2 during adsorption.[22] A schematic grafting procedure is shown in Scheme 1. Fig. 3 shows the synthesized support MCM-41 (2.2 nm), SBA-15 (6.6 nm) and KIT-6 (6.6 nm) have different pore sizes. All the mesoporous silica enriches with surface silanol groups and participates in grafting reaction. In anhydrous grafting, aminosilane directly reacts with surface silanol groups by condensation reaction (Scheme 1b) and grafted over the surface. However, lower adsorption capacity of M20T is possibly for lower amine loading for smaller pore size of MCM-41 as reflected from Table 1.

TMPTA is highly sensitive to moisture. In the presence of water, TMPTA forms a cluster *via*. hydrolysis reaction.[53] However, water also gets adsorbed on the negatively charged siloxane bridge of mesoporous silica and raptures the surface.[54] In this process, it creates new surface silanol groups on the surface, which also promote the aminosilane grafting capacity. The q_e of the aqueous grafted adsorbents are summarized in Table 2 and the grafting mechanism is shown in Scheme 1c. The higher accumulation of aminosilane in WM20T, WS20T and WK10T is the combined effect of increment in surface silanol groups and hydrolysis reaction between aminosilanes. During grafting, aminosilane forms a cluster in internal surface of the adsorbents.[53] The q_e of WM20T and WS20T was reduced, however increased in WK10T, even though after, the aminosilane loading was increased in all the adsorbents as analyzed by TG analysis. The increments in aminosilane loading are also understood by reduction in surface area and pore volume (Table 1).

The structure and pore size of the support plays an important role in the performance of adsorbent. The reduction in adsorption capacity can be correlated with the support structure and pore opening. During aqueous aminosilane grafting, pore of the hexagonal mesoporous silica MCM-41 and SBA-15 was blocked by aminosilane condensation reaction as shown in Scheme 1c and become a nonporous adsorbent as was also observed by N_2 adsorption/desorption analysis (pore volume becomes zero). The approximately same q_e of WM20T (0.64 mmol CO_2/g) and WS20T

(0.62 mmol CO_2/g) corroborates the above statement. During grafting in KIT-6, TMPTA forms a cluster in the channels by condensation and enhances the aminosilane loading. But it does not block the channels during grafting and enhanced CO_2 adsorption capacity by increasing the active amine sites. The enhancement in q_e of WK10T is the consequence of the above fact.

Reusability performance of adsorbents

In order to have practical applicability, stable sorption capacity in cyclic use is a primary criterion of a good adsorbent. In the present study, 20 adsorption/desorption cycles were subjected over M20T, S20T, K30T and WK30T at 30 ºC. After each cycle of adsorption, samples were degassed at 95 ºC for an hour. All the adsorbents showed a stable sorption capacity till 20 cycles as shown in Fig 11. This indicates the stable attachment of aminosilane with the silica surface and no amine loss to the environment.[25]

4. Conclusion

A series of ordered mesoporous silica samples namely MCM-41, SBA-15 and KIT-6 were synthesized by liquid crystal template mechanism and functionalized with TMPTA in anhydrous and aqueous amine solution. The synthesized adsorbents were subjected to CO_2/N_2 adsorption at various conditions. The adsorption capacity of anhydrous grafted adsorbents was followed the order as K30T (1.89 mol CO_2/kg) > S20M (1.54 mol CO_2/kg) > M20T (1.36 mol CO_2/kg) at 30 ºC and 1 bar. Moreover, adsorption capacity was increased to 2.59 mol CO_2/g after aqueous grafting over KIT-6. The CO_2/N_2 selectivity of the KIT-6 based adsorbent is much higher than MCM-41 and SBA-15. The lower adsorption capacity as well as selectivity of TMPTA grafted MCM-41 and SBA-15 makes them less favourable in particle application. In addition to CO_2 adsorption, WK30T is easily regenerable at moderate temperature and showed good stability for several adsorption/adsorption cycles. Intermolecular condensation of aminosilane blocks the pores and thereby reduces the CO_2 sorption capacity of TMPTA grafted MCM-41 and SBA-15. However,

presence of interconnected channels in KIT-6 eliminates that possibility and made the TMPTA grafted KIT-6 with high CO_2 adsorption capacity and excellent CO_2/N_2 selectivity a potential adsorbent for commercial application.

Acknowledgements

The authors would like to acknowledge Central Instrument Facility (CIF) of Indian Institute of technology Guwahati (IITG) for Nitrogen adsorption/desorption analysis at –196 °C, CO_2/N_2 adsorption analysis, FESEM and TEM analysis.

Electronic Supplementary Information

The effect of TMPTA concentration (Fig. S1) and TG analysis (Fig. S2) are available in ESI.

References

[1] Annual energy outlook 2015 with projections to 2040. (http://www.eia.gov/forecasts/aeo/)

[2] F. M. Orr, Jr., CO_2 capture and storage: are we ready? *Energy Environ. Sci.*, 2009, **2**, 449–458.

[3] P. Markewitz, W. Kuckshinrichs, W. Leitner, J. Linssen, P. Zapp, R. Bongartz, A. Schreibera and Thomas E. Müller, *Energy Environ. Sci.,* 2012, **5**, 7281–7305.

[4] R. Idem, M. Wilson, P. Tontiwachwuthikul, A. Chakma, A. Veawab, A. Aroonwilas, and D. Gelowitz, *Ind. Eng. Chem. Res.*, 2006, **45**, 2414–2420.

[5] O. Cheung and N. Hedin, *RSC Adv.*, 2014, **4**, 14480–14494.

[6] S. García, J. J. Pis, F. Rubiera, and C. Pevida, *Langmuir*, 2013, **29**, 6042−6052.

[7] D. Lin, X. Zhang, X. Cui, and W. Chen, *RSC Adv.*, 2014, **4**, 27414–27421.

[8] J. A. Mason, T. M. McDonald, T.-H. Bae, J. E. Bachman, K. Sumida, J. J. Dutton, S. S. Kaye, and J. R. Long, *J. Am. Chem. Soc.*, 2015, **137**, 4787−4803.

[9] S. Xiang, Y. He, Z. Zhang, H. Wu, W. Zhou, R. Krishna, and B. Chen, *Nat. Commun.*, 2012, **3**, 954.

[10] J. Peng, S. Xian, J. Xiao, Y. Huang, Q. Xia, H. Wang, Z. Li, *Chem. Eng. J.*, 2015, **270**, 282–289.

[11] Z. Zhang, Z.–Z. Yao, S. Xiang and B. Chen, *Energy Environ. Sci.*, 2014, **7**, 2868–2899.

[12] P. Mishra, S. Edubilli, B. Mandal, and S. Gumma, *J. Phys. Chem. C* 2014, **118**, 6847−6855.

[13] H. A. Patel, F. Karadas, A. Canlier, J. Park, E. Deniz, Y. Jung, M. Atilhan, and C. T. Yavuz, *J. Mater. Chem.*, 2012, **22**, 8431–8437.

[14] J. Wang, J. Huang, X. Wu, B. Yuan, Y. Sun, Z. Zeng, and S. Deng, *Chem. Eng. J.,* 2014, **256**, 390–397.

[15] F. Karadas, C. T. Yavuz, S. Zulfiqar, S. Aparicio, G. D. Stucky, and M. Atilhan, *Langmuir*, 2011, **27**, 10642–10647.

[16] S. C. Lee, B. Y. Choi, T. J. Lee, C. K. Ryu, Y. S. Ahn and J. C. Kim, *Catal. Today*, 2006, **111**, 385–390.

[17] S. C. Lee, H. J. Chae, S. J. Lee, Y. H. Park, C. K. Ryu, C. K. Yi, and J. C. Kim, *J. Mol. Catal. B: Enzym.,* 2009, **56**, 179–184.

[18] A. Zhao, A. K. Samanta, P. Sarkar, and R. Gupta, *Ind. Eng. Chem. Res.*, 2013, **52**, 6480−6491.

[19] T. Yokoi, H. Yoshitake and T. Tatsumi, *J. Mater. Chem.*, 2004, **14**, 951–957.

[20] N. Mittal, A.K. Samanta, P. Sarkar and R. Gupta, *Energy Sci. Eng.*, 2015, **3**, 207 – 220.

[21] N. Hiyoshi, K. Yogo, and T. Yashima, *Microporous Mesoporous Mater.*, 2005, **84**, 357–365.

[22] L. Wang and R. T. Yang, *J. Phys. Chem. C*, 2011, **115**, 21264–21272.

[23] M. R. Mello, D. Phanon, G. Q. Silveira, P. L. Llewellyn, and C. M. Ronconi, *Microporous Mesoporous Mater.*, 2011, **143**, 174–179.

[24] M. Gil, I. Tiscornia, Ó. de la Iglesia, R. Mallada, and J. Santamaría, *Chem. Eng. J.,* 2011, **175**, 291–297,

[25] N. N. Linneen, R. Pfeffer, and Y. S. Lin, *Chem. Eng. J.,* 2014, **254**, 190–197.

[26] T. C. Santos, S. Bourrelly, P. L. Llewellyn, J. W. M. Carneiro and C. M. Ronconi, *Phys. Chem. Chem. Phys.*, 2015, **17**, 11095–11102.

[27] Y. G. Ko, S. S. Shin, and U. S. Choi, *J. Colloid Interface Sci.*, 2011, **361**, 594–602.

[28] R. Kishor, and A. K. Ghoshal, *Chem. Eng. J.*, 2015, **262**, 882–890.

[29] V. Zeleňák, M. Badaničová, D. Halamová, J. Čejka, A. Zukal, N. Murafa, and G. Goerigk, *Chem. Eng. J.*, 2008, **144**, 336–342.

[30] J. S. Beck, J. C. Vartuli, W. J. Roth, M. E. Leonowicz, C. T. Kresge, K. D. Schmitt, C. T-W. Chu, D. H. Olson, E. W. Sheppard, S. B. McCullen, J. B. Higgins, and J. L. Schlenker, *J. Am. Chem. Soc.*, 1992, **114**, 10834–10843.

[31] J. Zhao, F. Simeon, Y. Wang, G. Luo and T. A. Hatton, *RSC Adv.*, 2012, **2**, 6509–6519.

[32] D. S. Dao, H. Yamada, and K. Yogo, *Ind. Eng. Chem. Res.*, 2013, **52**, 13810−13817.

[33] C. K. P. Neeli, S. Ganji, V. S. P. Ganjala, S. R. R. Kamaraju and D. R. Burri, *RSC Adv.*, 2014, **4**, 14128–14135.

[34] J. Feng, Z. Wang, B. Shen, L. Zhang, X. Yanga and N. He, *RSC Adv.*, 2014, **4**, 28683–28690.

[35] M. Vallet-Regi, A. Rámila, R. P. d. Real, and J. Pérez–Pariente, *Chem. Mater.*, 2001, **13**, 308–311.

[36] P. J. E. Harlick, and A. Sayari, *Ind. Eng. Chem. Res.*, 2007, **46**, 446–458.

[37] S. Loganathan, M. Tikmani, and A. K. Ghoshal, *Langmuir*, 2013, **29**, 3491–3499.

[38] X. Yan, S. Komarneni, and Z. Yan, *J. Colloid Interface Sci.*, 2013, **390**, 217–224.

[39] W.–J. Son, J.–S. Choi, and W.–S. Ahn, *Microporous Mesoporous Mater.*, 2008, **113**, 31–40.

[40] M. Kruk and M. Jaroniec, *Chem. Mater.* 2001, **13**, 3169–3183.

[41] X. S. Zhao, G. Q. Lu, A. K. Whittaker, G. J. Millar, and H. Y. Zhu, *J. Phys. Chem. B*, 1997, **101**, 6525–6531.

[42] V. Zelenak, D. Halamova, L. Gaberova, E. Bloch, and P. Llewellyn, *Microporous Mesoporous Mater.*, 2008, **116**, 358–364.

[43] C. S. Srikanth, and S. S. C. Chuang, *J. Phys. Chem. C*, 2013, **117**, 9196 – 9205.

[44] Q. Wu, S. Chen and H. Liub, *RSC Adv.*, 2014, **4**, 27176–27183.

[45] Y. Belmabkhout, G. D. Weireld, and A. Sayari, *Langmuir* 2009, **25**, 13275–13278

[46] R. Sanz, G. Calleja, A. Arencibia, and E. S. Sanz-Pérez, *Microporous Mesoporous Mater.*, 2012, **158**, 309–317.

[47] G. P. Knowles, S. W. Delaney, and A. L. Chaffee, *Ind. Eng. Chem. Res.*, 2006, **45**, 2626–2633.

[48] L. Zhou, J. Fan, G. Cui, X. Shang, Q. Tang, J. Wang, and M. Fan, *Green Chem.*, 2014, **16**, 4009–4016.

[49] Y. Belmabkhout and A. Sayari, *Energy Fuels*, 2010, **24**, 5273–5280.

[50] M. G. Rabbani, T. E. Reich, R. M. Kassab, K. T. Jackson and H. M. El-Kaderi, *Chem. Commun.*, 2012, **48**, 1141–1143.

[51] J.–R. Li, R. J. Kuppler and H.–C. Zhou, *Chem. Soc. Rev.*, 2009, **38**, 1477–1504.

[52] J.–X. Hu, H. Shang, J.–G. Wang, L. Luo, Q. Xiao, Y.–J. Zhong, and W.–D. Zhu, *Ind. Eng. Chem. Res.*, 2014, **53**, 11828−11837.

[53] C.–H. Chiang, N.–I Liu, and J. L. Koenig, *J. Colloid Interface Sci.*, 1982, **86**, 26–34.

[54] T. A. Michalske and S. W. Freiman, *Nature*, 1982, **295**, 511–512.

Table with captions

Table 1. Textural and structural properties of the TMPTA grafted OMSs

OMSs	S_{BET} (m^2/g)	v_t (cc/g)	d_{BJH} (nm)
MCM-41	1492	0.91	2.2
M15T	107	0.16	2.1
M20T	82	0.16	1.6
M25T	77	0.16	1.6
WM20T	31	0.005	1.6
SBA-15	857	1.23	6.6
S15T	321	0.57	4.9
S20T	301	0.53	4.9
S25T	281	0.50	4.9
WS20T	24	0.007	1.35
KIT-6	860	1.24	6.6
K20T	316	0.61	5.6
K25T	312	0.61	5.6
K30T	310	0.59	5.6
K35T	305	0.59	5.6
WK30T	190	0.36	4.9
WK30T	55	0.12	4.3

S_{BET}: Specific surface area, v_t: Pore volume, d_{BJH}: Pore diameter

Table 2. Summary of TMPTA grafted OMSs CO_2 adsorption performance.

OMSs	dp (nm)	Adsorption condition (ºC / bar)	Adsorption capacity (mol CO_2/kg)	Methods	Reference
MCM-41	2.7	30/ 1	1.01	Manometric gas dosing system	[26]
PE-MCM-41	11.7	25/1	2.50†	Gravimetric	[45]
SBA-15	8.9	45/1	1.8	Gravimetric	[46]
HMS	2.21	20/1bar	1.1	TGA/DTA	[47]
Silica aerogels	42.7	25C/1bar	2.61†	Electro-microbalance	[25]
SBA-15-p	14.7	25C/1bar	2.67	Volumetric	[48]
SBA-15-f	7.5	25C/1bar	1.23	Volumetric	[48]
MCM-41 (M20T)	2.2	30C/1bar	1.36	Volumetric	Present study
SBA-15 (S20T)	6.6	30C/1bar	1.54	Volumetric	Present study
KIT-6 (K30T)	6.6	30C/1bar	1.89	Volumetric	Present study
KIT-6 (WK30T)	6.6	30C/1bar	2.59†	Volumetric	Present study

† **:** Aqueous grafting

Table. 3 Comparisons of TMPTA grafted OMSs as adsorbent.

OMSs	q_e (mol CO_2/kg)		(mol N/kg)	% amine efficiency	Selectivity at	ΔE_{ads} (kJ/mol)
	30 ºC	60 ºC		mol(CO_2)/mol(N)	30 ºC	
MCM-41	0.56	0.39	—	—	14	18
SBA-15	0.74	0.48	—	—	23	20
KIT-6	0.64	0.40	—	—	15	18
M20T	1.36	1.14	3.72	36.6	491	31
WM20T	0.67	—	4.70	14.2	—	—
S20T	1.54	1.18	3.98	38.7	635	67
WS20T	0.63	—	5.46	8.7	—	—
K30T	1.89	1.73	4.25	44.8	793	42
WK30T	2.59	2.38	5.73	45.1	873	33

q_e: Equilibrium adsorption capacity at 1 bar; Selectivity: Calculated at 0.15:0.85 partial pressure ratio, ΔE_{ads}: Enthalpy of adsorption

Scheme with captions

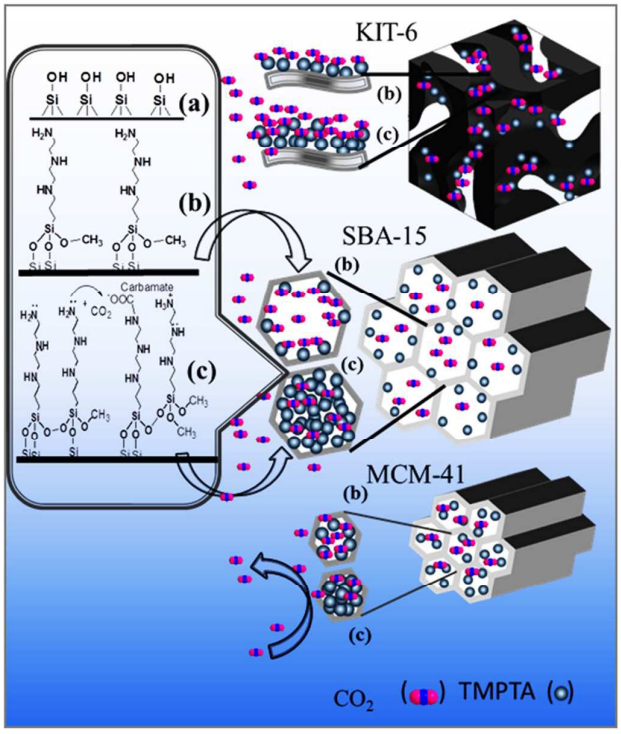

Scheme 1. Grafting mechanism of aminosilane in different mesoporous silica MCM-41, SBA-15 and KIT-6

Figure with captions:

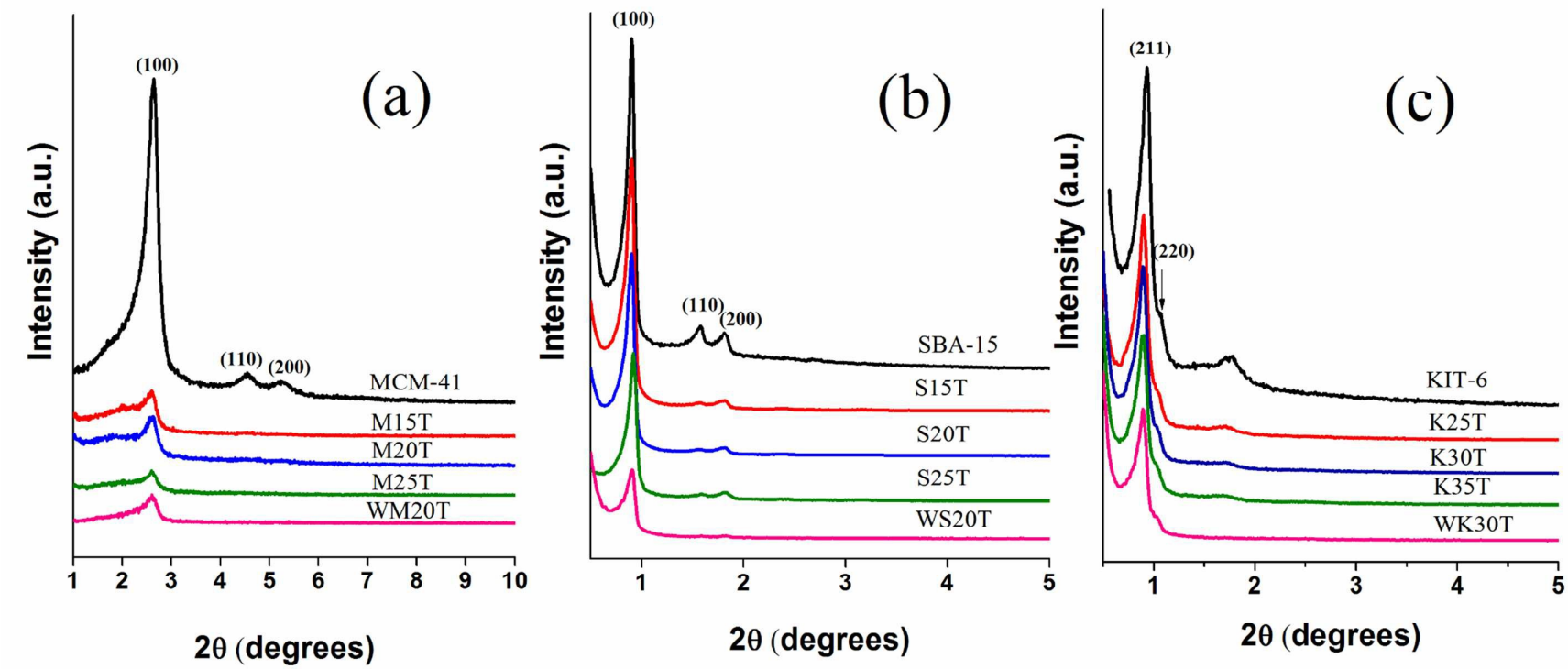

Fig. 1 X-ray diffraction pattern of ordered mesoporous silica before and after TMPTA grafting on (a) MCM-41 (b) SBA-15 and (c) KIT-6 adsorbents.

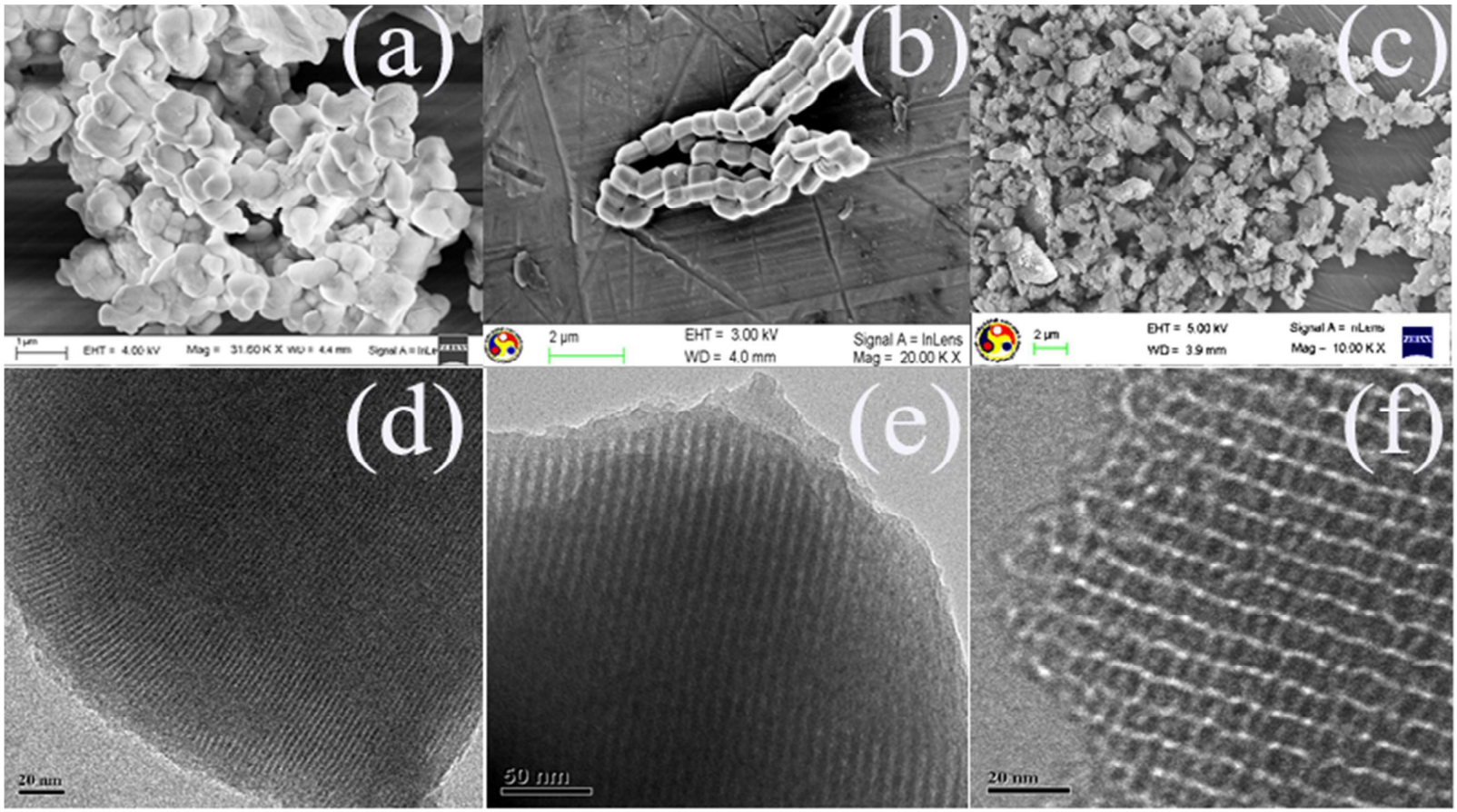

Fig. 2 FESEM micrograph of (a) MCM-41 (b) SBA-15, (c) KIT-6 and TEM micrograph of (d) MCM-41 (e) SBA-15 and (f) KIT-6 mesoporous silica.

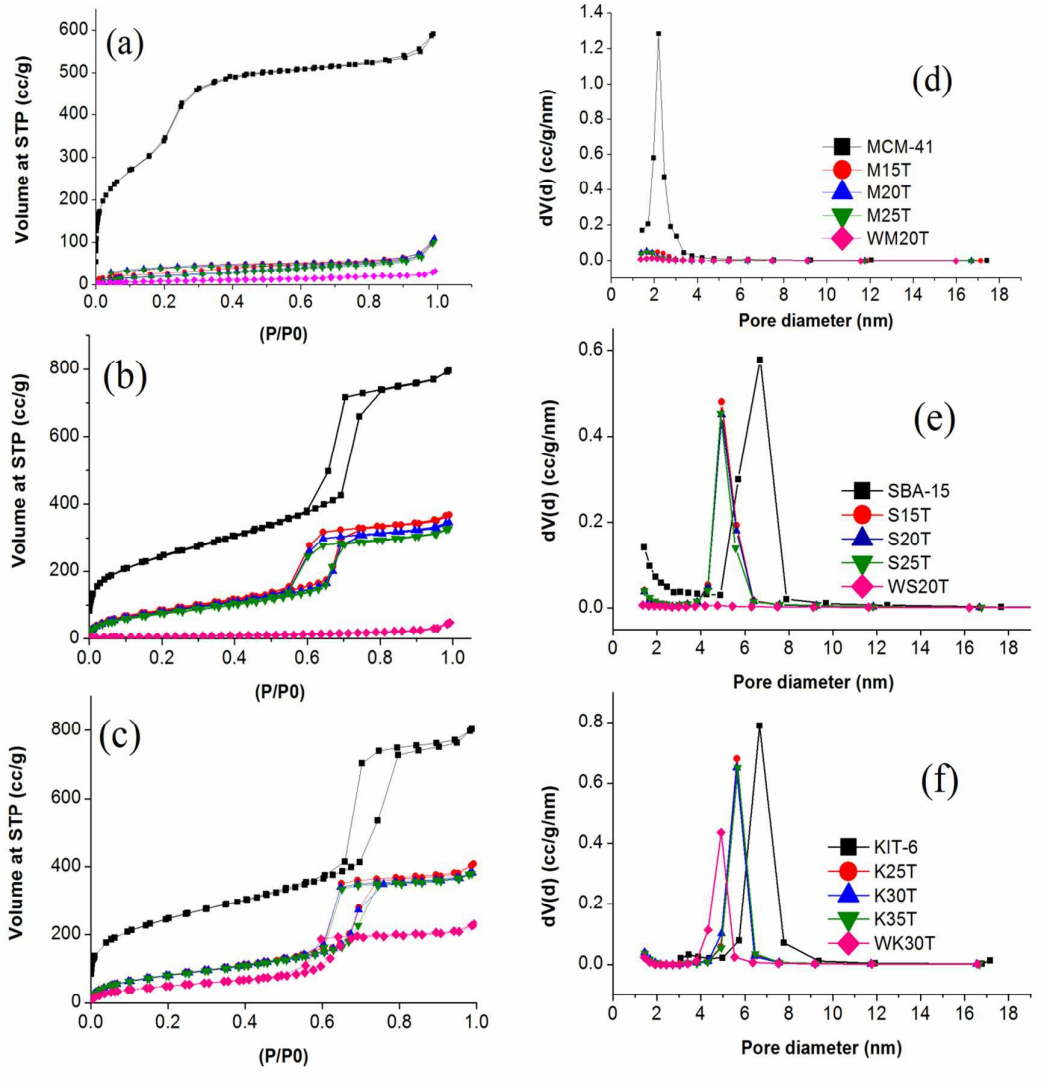

Fig. 3 Nitrogen adsorption/desorption of before and after aminosilane grafting of (a) MCM-41 (b) SBA-15, (c) KIT-6 at –196 °C and pore size distribution of (d) MCM-41 (e) SBA-15 and KIT-6 adsorbents.

\

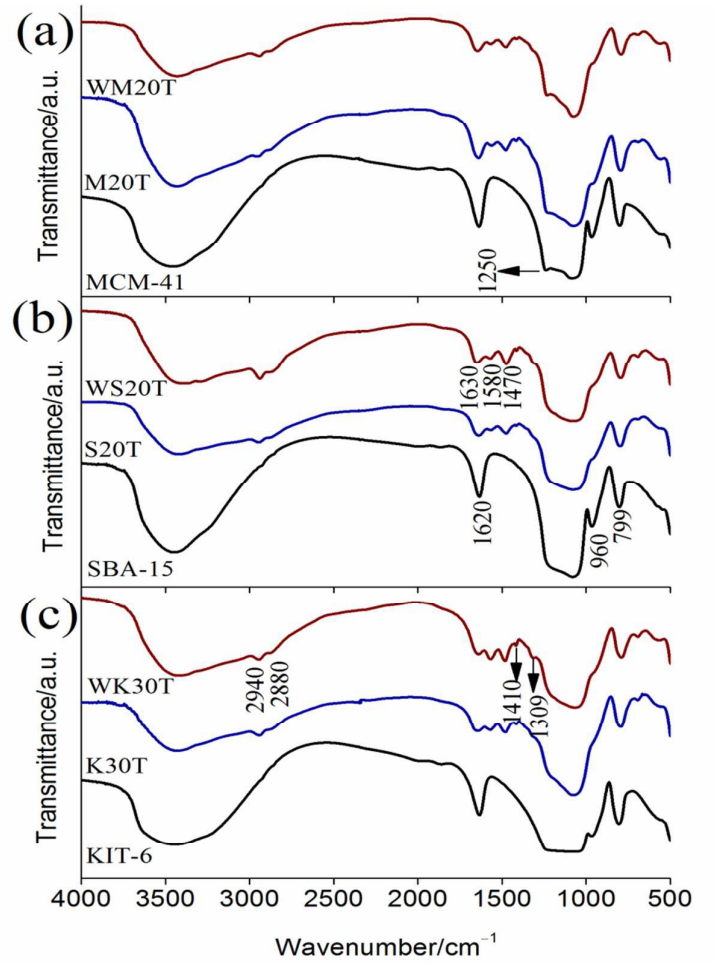

Fig. 4 IR-spectra of pure and TMPTA grafted (a) MCM-41 (b) SBA-15 and (c) KIT-6.

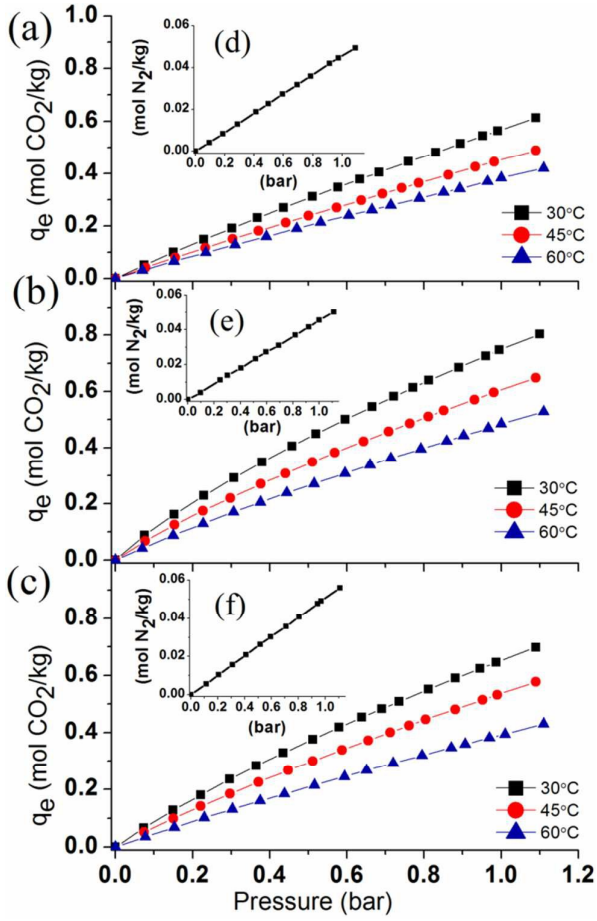

Fig. 5 CO_2 adsorption on (a) MCM-41, (b) SBA-15, and (c) KIT-6 and corresponding N_2 adsorption in (d), (e) and (f), respectively at 30°C.

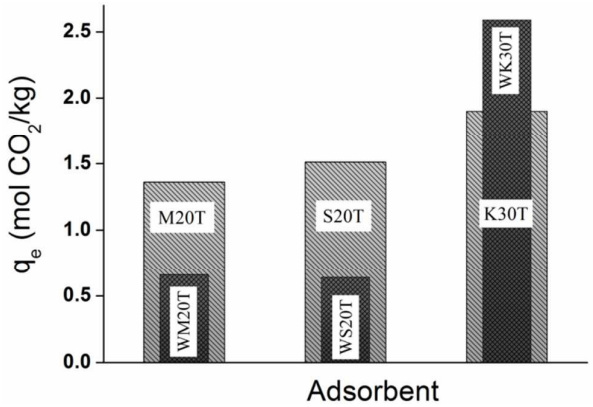

Fig. 6 Effect of water used in aminosilane grafting and CO_2 adsorption capacity.

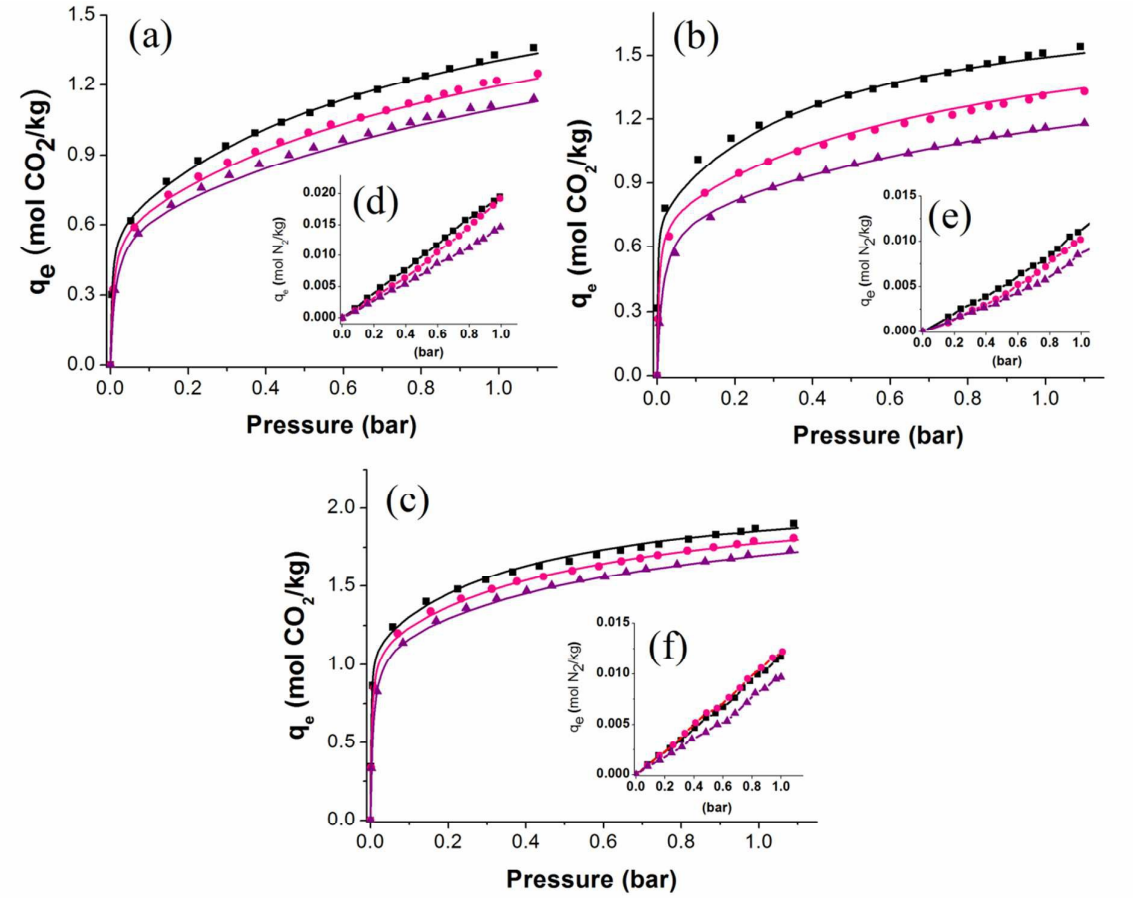

Fig. 7 CO_2 adsorption isotherms for (a) M20T (b) S20T and (c) K30T and N_2 adsorption isotherm in (d) M20T, (e) S20T and (f) K30T at different temperatures (■: 30 ºC) (●: 45 ºC) and (▲: 60 ºC).

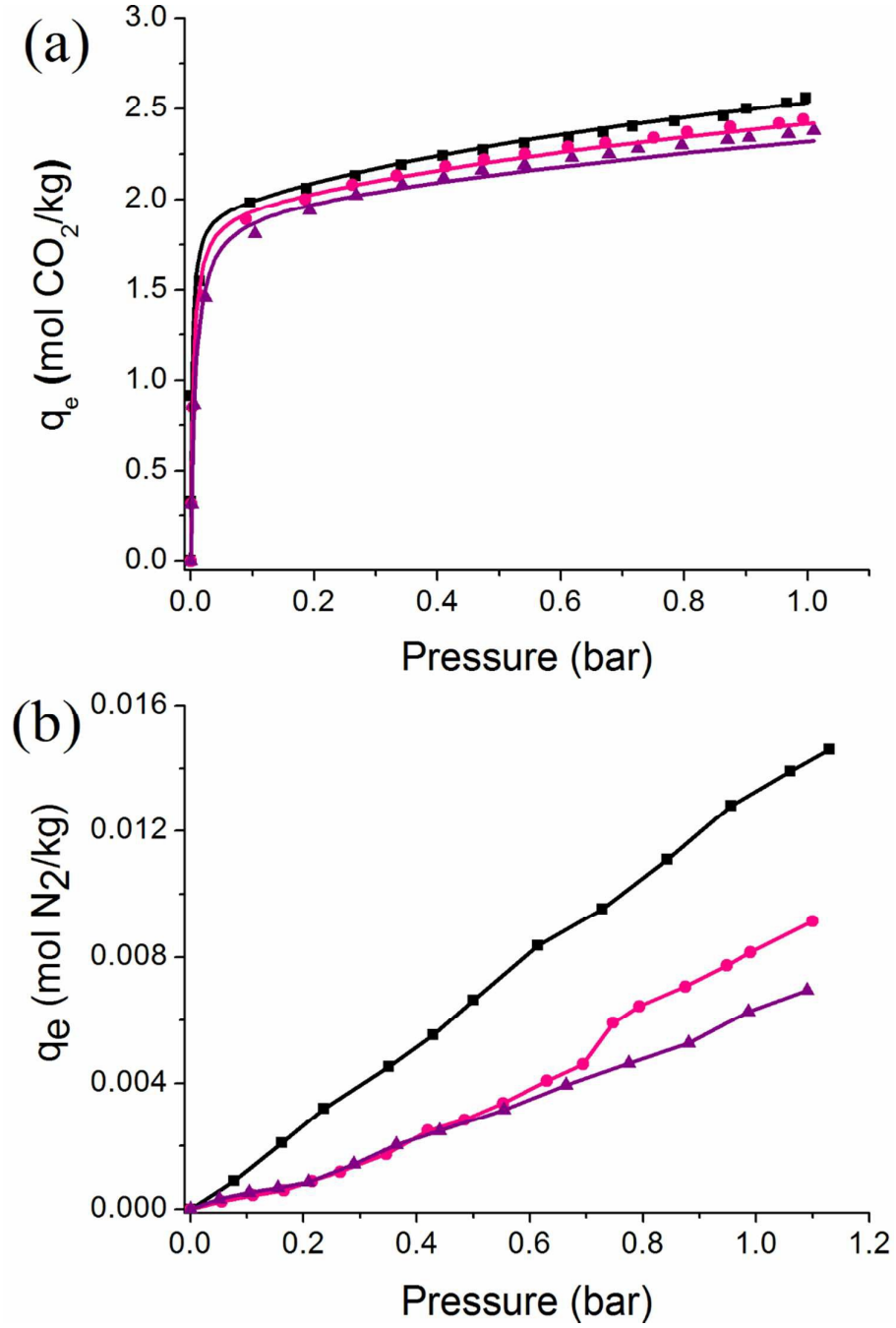

Fig. 8 (a) CO_2 and (b) N_2 adsorption isotherms on WK30T at different temperatures (■: 30 ºC) (●: 45 ºC) and (▲: 60 ºC)

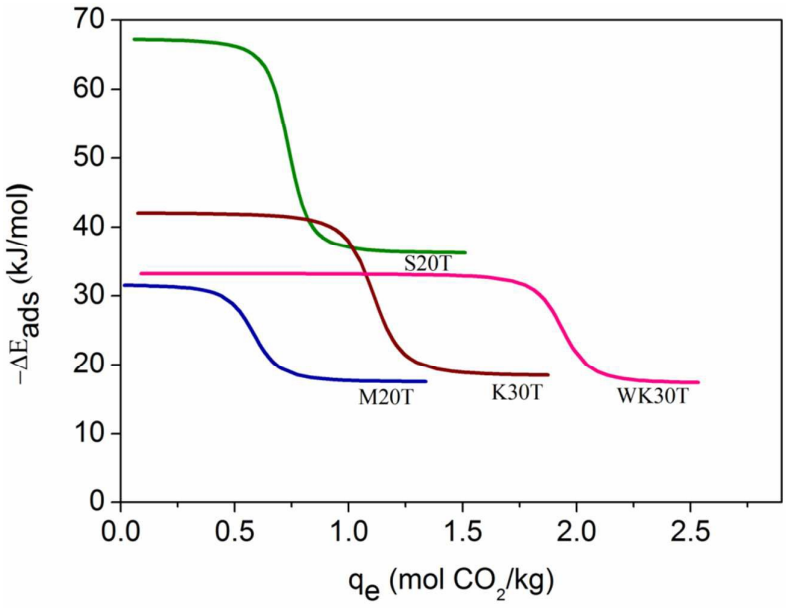

Fig. 9 Enthalpy curve of CO_2 adsorption over (a) M20T, (b) S20T, (c) K30T and (d) WK30T adsorbents

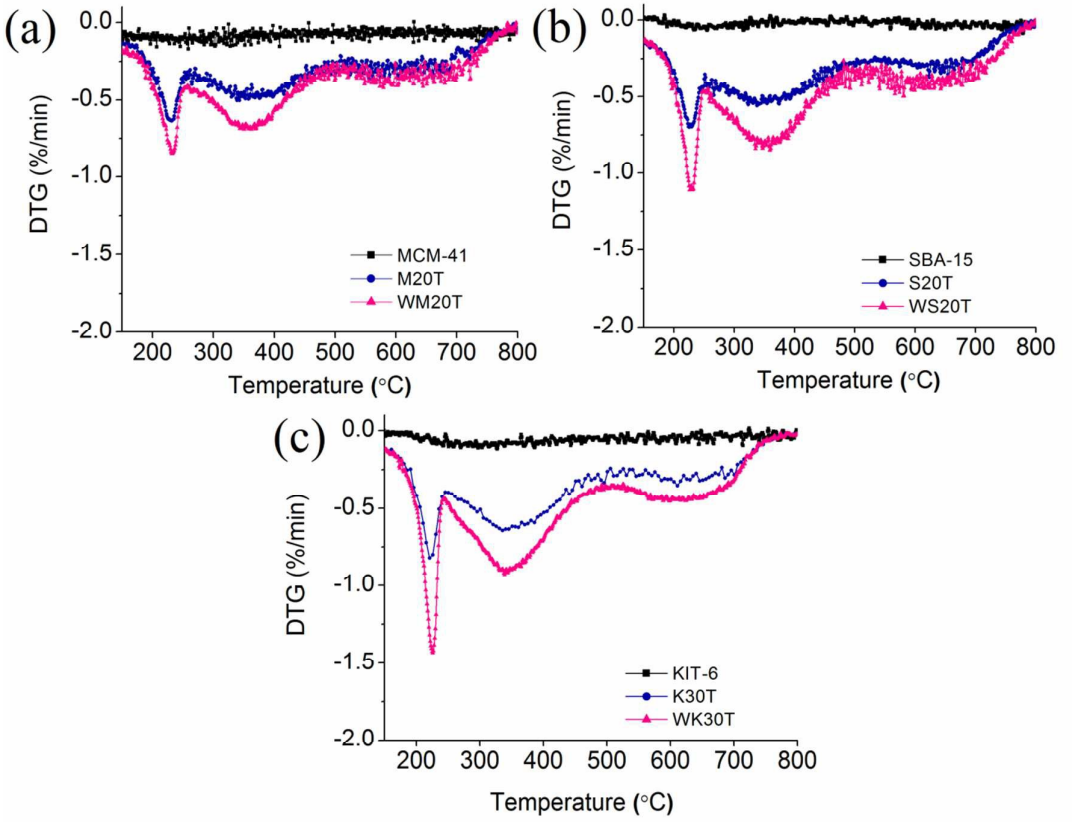

Fig. 10 Differential thermal gravimetric (DTG) analysis of pure and TMPTA grafted (a) MCM-41 (b) SBA-15 and (c) KIT-6 mesoporous silica.

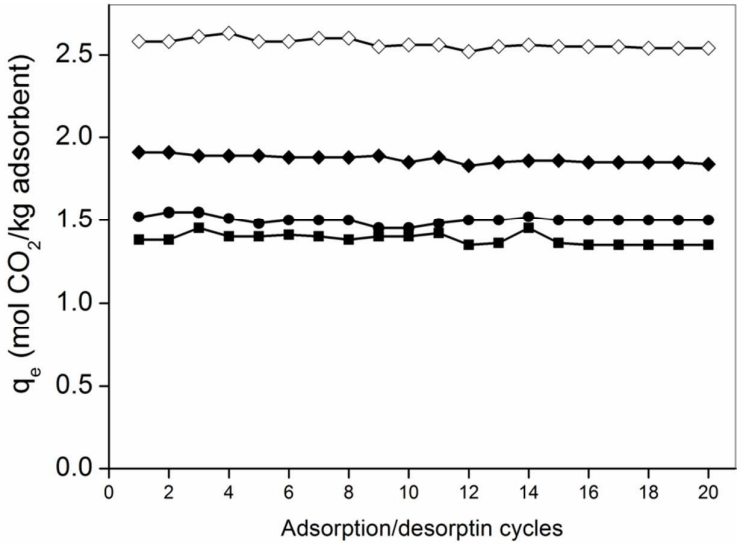

Fig. 11 Cyclic performance of TMPTA grafted M20T (■), S20T (●), K30T (♦) and WK30T (◊) adsorbents

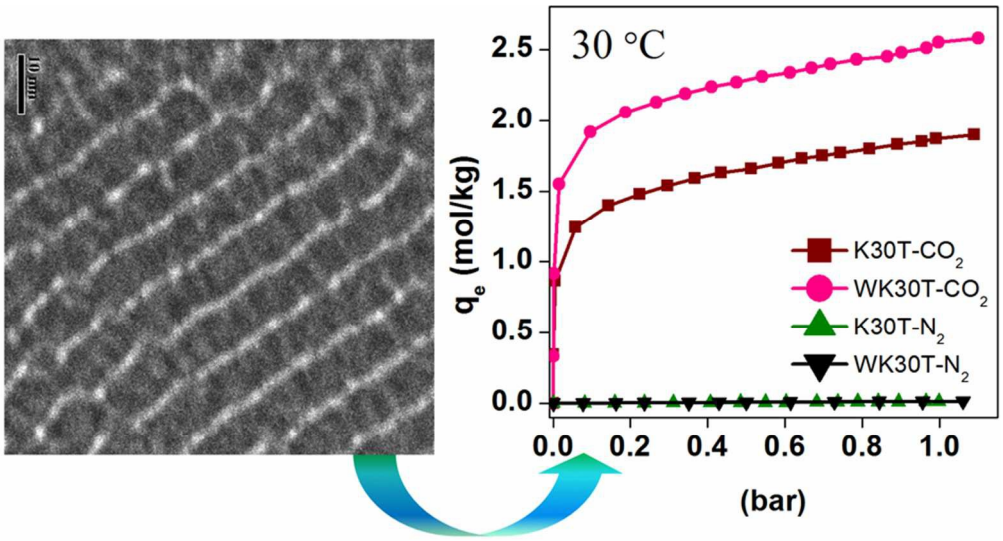

80x43mm (300 x 300 DPI)